Supporting Information

Blancing the Mechanical, Electronic, and Self-healing Properties in Conductive Self-Healing Hydrogels for Wearable Sensor Applications

Gehong Su,[a,b] Shuya Yin,[a] Youhong Guo,[b] Fei Zhao,[b] Quanquan Guo,[a] Xinxing Zhang,[a] Tao Zhou,[a,] and Guihua Yu[b,]**

[a] State Key Laboratory of Polymer Materials Engineering of China, Polymer Research Institute, Sichuan University, Chengdu 610065, China;

[b] Materials Science and Engineering Program, Texas Materials Institute, The University of Texas at Austin, Austin, TX 78712, USA

*Corresponding authors. E-mail address: zhoutaopoly@scu.edu.cn (T. Zhou); ghyu@austin.utexas.edu (G. Yu)

Table of contents

S1. Experimental Section

Materials. Acrylic acid (AA), lauryl methacrylate (LMA), and hexadecyl trimethyl ammonium bromide (CTMAB) were purchased from Adamas-beta®. Aniline (ANI, ≥99.5%), pyrrole (PPy, 99%), phytic acid (PA, 50 wt% in water), and ammonium persulfate (APS) were brought from Sigma-Aldrich. Urea was purchased from Chengdu Kelong Chemical Reagent Company (China). All the chemical reagents were used as received without further purification. The stretchable tape (VHB4905) was purchased from 3M.

Synthesis of HAPAA hydrogel. The self-healable HAPAA/PANI hydrogels were synthesized via a two-step method. The first step is the synthesis of the HAPAA hydrogel *via* micellar polymerization. The detailed composition of the HAPAA hydrogels with different AA concentrations was listed in Table S1. In a typical synthesis, a certain amount of hydrophilic monomer AA, the hydrophobic monomer LMA, and the surfactant CTMAB were dissolved in a certain amount of deionized water (the total mass of all formulations was fixed at 20 g to achieve a reasonable comparison), and then stirred for 4 hours to obtain a homogeneous solution. After that, the initiator APS (0.5 wt.% relative to the total mass of AA and LMA) was added into the solution and keep stirring for 5 mins. Subsequently, the precursor solution was poured into home-made reaction equipment which was assembled by two rectangle-shaped glass plates and a hollow silicon rubber spacer (the dimension of the hydrogel can be tuned by adjusting the size of the glass plate and the thickness of the spacer). Then, the sealed reaction equipment was placed at 60 °C for 6 hours. After polymerization, the HAPAA hydrogel can be peeled off from the plate. Then, the dehydrated HAPAA hydrogel was obtained by placing the purified HAPAA hydrogel in the open air for 48 h.

Synthesis of PAAN hydrogels. The PAAN conductive hydrogel was synthesized according to the following procedure. Firstly, a certain amount of ANI and PA was mixed with 50 mL deionized water and then sonicated (250W) for 5 mins to make sure the ANI is fully dissolved. Afterward, the dehydrated HAPAA hydrogel was immersed in ANI/PA solution to be swelled again. After the hydrogel reaches its original weight before drying, it was immersed into the pre-cooled APS/PA aqueous solution to start the polymerization at ~4 °C for 24 h to obtain the conductive PAAN hydrogel. For convenience, the PAAN hydrogels with different AA and PANI contents were denoted as PA_xAN_y hydrogel, x represents the AA weight ratio in the HAPAA network, and y represents the ANI concentration (M) in the PANI precursor solution. For example, $PA_{25}AN_{0.15}$ hydrogel means the AA content in HAPAA hydrogel is 25.0 wt.%, and the concentration of the ANI monomer in the ANI/PA precursor solution is 0.15 M.

Characterizations. The water content was measured by drying a piece of the as-synthesized hydrogel in a 60 °C oven until the weight reaches constant, the water content can be calculated as $(W_0 - W_d)/W_0 \times 100\%$, in which W_0 is the weight before drying, and W_d is the weight after drying. For the swelling ratio test, the dried hydrogel sample was placed in distilled water at room temperature and removed from the water at regular time intervals. The hydrogels' weight was recorded after wiping off the water on the gel surface with a filter paper. The swelling ratio can be calculated as $(M_t - M_0)/M_0$, where M_t is the mass of the

swollen hydrogels at time t, and M_0 is the mass of the dried sample. Attenuated total reflection infrared (ATR-FTIR) spectra in the wavenumber region of 500-4000 cm^{-1} were collected by a Nicolet iS50 spectrometer (USA) equipped with a deuterated triglycine sulfate (DTGS) detector and an ATR accessory with a ZnSe IRE-ATR crystal at a resolution of 4 cm^{-1} with 20 scans. The XRD pattern was measured via a powder X-ray diffractometer (Ultima IV, Rigaku) with Cu Ka radiation operating at 40 kV and 40 mA. The microstructure of the hydrogels was observed by a scanning electron microscope (SEM, JEOL, JSM-5900LV, Japan). The sample was freeze-dried for 48 hours coated with a thin layer of gold before taking SEM images. Rheological experiments of the hydrogels were carried out by a AR 2000EX rheometer (TA instrument) using a parallel plate on a Peltier plate in a frequency sweep mode from 0.1 to 100 rad s^{-1} at a fixed strain of 1% at room temperature. Laser confocal microscopy (LCSM, LSM700 Carl Zeiss, German) was performed to observe the morphology of the sample after cutting and healing (Laser wavelength is 405 nm, the laser intensity is 5, and pinhole diameter is 1 Å). The electrical conductivity of HAPAA and PAAN hydrogels was tested by a four-point probe tester (ST-2258A, China) with a linear probe head at room temperature. The conductivity (σ) was calculated by the results from the measurement of sheet resistance (R_s) and thickness (t) according to the following equation: $\sigma = 1/R_s t$. The resistance change signals of the sensors were collected in real-time by using a Keithley 2601B source meter (USA).

Mechanical test. All the mechanical tests (tensile and compression) were conducted on a versatile testing machine (Instron 5567, USA) with a 1 kN load cell at room temperature. The tensile tests were performed with the dumbbell-like samples (2 mm in thickness, 4 mm in width, and 50 mm in length) with a constant stretching speed of 100 mm/min. The compression tests were carried out with cylinder samples (about 14 mm in diameter) at a fixed compressing speed of 3 mm/min. The tensile strain (ε) was defined as the ratio of the gauge length (L) to the initial gauge length (L_0, 20 mm in this work) ($\varepsilon=(L-L_0)/L_0$), and the tensile stress (σ) is calculated by dividing the force (F) by the initial cross-section area (A_0) of the sample ($\sigma=F/A_0$). The elastic modulus (E) was calculated from the slope of the initial linear region of the stress-strain curve (0-25% strain for tensile and 0-35% for compression). The toughness (T) was calculated from the area under the stress-strain curve based on the following equation:

$$T = \int_{\varepsilon_0}^{\varepsilon_f} \sigma(\varepsilon) d\varepsilon$$

Where ε_0 and ε_f represent the initial strain before stretch and the strain at break, respectively. The cyclic tensile and compression tests were conducted with no time interval between two adjacent cycles.

Self-healing tests. To evaluate the self-healing ability of PAAN hydrogels, a dumbbell-shaped hydrogel sample was completely cut into two halves at first. Then, these two halves were connected with each other and placed at room temperature (~25°C) with high relative humidity (~70%) to minimize the water loss during self-healing. After healing, the samples with a weight decrease of less than 3% were used for the tensile test to evaluate the self-healing efficiency.

Fabrication of the sensors. To assemble the strain sensor, the hydrogel film was cut into the strip-like sample with different dimensions (40 × 5 × 2 mm for large-scale body movement detection, 25 × 5 × 2 mm for pronunciation detection). Then, two individual copper wires were wrapped around both ends of the strip sample, and then two double-sided conductive flexible copper tapes were tightly wrapped on the wires to obtain a stable signal output. After that, stretchable VHB tapes were used to encapsulate the strip samples to prevent the water from evaporation. To obtain a pressure sensor, the hydrogel film was cut into rectangle-like samples (3 mm in thickness) at first. Afterward, two conductive copper wires were tightly adhered to the opposite ends of the gel sample to assemble electrodes. Finally, two pieces of VHB tapes were utilized to encapsulate the gel sample into a sandwich-like pressure sensor. Note that, before encapsulation, each surface of the gel was slightly wiped by ethanol and then dried with N_2 for 2 min to remove water from the gel surface to improve the adhesion among the gel, copper tapes, and VHB tapes.

S2. Supporting Tables

Table S1. Compositions of the HAPAA hydrogels with different AA mass ratios.

Mass ratio of AA	AA (g)	LMA (g)	CTAB (g)	H_2O (g)	Total (g)
20.0%	4.000	0.267	0.600	15.133	20.000
22.5%	4.500	0.300	0.680	14.520	20.000
25.0%	5.000	0.333	0.750	13.920	20.000
27.5%	5.500	0.367	0.825	13.308	20.000

Table S2. The mechanical properties of HAPAA and $PA_{25}AN_y$ hydrogels with different ANI concentrations.

	HAPAA	**$PA_{25}AN_{0.10}$**	**$PA_{25}AN_{0.15}$**	**$PA_{25}AN_{0.20}$**	**$PA_{25}AN_{0.30}$**
σ_t (MPa)[a)]	0.30 ± 0.02	0.72 ± 0.02	0.85 ± 0.05	0.68 ± 0.06	0.42 ± 0.09
ε (%)[b)]	2747 ± 117	2672 ± 92	2503 ± 82	1533 ± 88	1060 ± 120
E_t (KPa)[c)]	5.75 ± 0.4	48.90 ± 2.7	52.25 ± 2.5	62.37 ± 4.8	67.68 ± 4.2
T (MJ/m^3)[d)]	3.27 ± 0.26	7.48 ± 0.67	7.85 ± 0.72	3.84 ± 0.60	1.80 ± 0.51
σ_c (MPa)[e)]	0.56 ± 0.05	4.72 ± 0.19	5.51 ± 0.31	6.22 ± 0.25	8.23 ± 0.28
E_c (KPa)[f)]	51.35 ± 4.2	66.80 ± 3.7	83.59 ± 5.1	106.42 ± 6.2	139.30 ± 10.4
Γ **($J\ m^{-2}$)**[g)]	3096 ± 288	4401 ± 510	4199 ± 262	2808 ± 354	2406 ± 366

Note: a) tensile stress; b) tensile strain; c) tensile modulus; d) toughness; e) compression stress; f) compression modulus; g) fracture energy.

Table S3. The mechanical properties of $PA_xAN_{0.15}$ hydrogels with different AA contents.

	$PA_{20}AN_{0.15}$	**$PA_{22.5}AN_{0.15}$**	**$PA_{25}AN_{0.15}$**	**$PA_{27.5}AN_{0.15}$**
σ_t (MPa)	0.37 ± 0.017	0.54 ± 0.035	0.85 ± 0.050	0.73 ± 0.056
ε (%)	2416 ± 52	2250 ± 70	2503 ± 82	1991 ± 81
E_t (KPa)	13.09 ± 1.5	25.05 ± 1.3	52.25 ± 2.5	62.40 ± 2.3
T (MJ/m^3)	2.95 ± 0.20	3.99 ± 0.38	7.85 ± 0.72	4.97 ± 0.59
σ_c (MPa)	1.06 ± 0.16	3.60 ± 0.30	5.51 ± 0.31	6.59 ± 0.44
E_c (KPa)	53.31 ± 2.26	78.49 ± 2.31	83.59 ± 5.1	99.72 ± 5.96

Table S4 Comparisons of the mechanical properties, self-healing performance, and sensory performance of our hydrogel with other recently reported hydrogel sensors.

Composition	Mechanical property						Sensitivity			Ref.
	Tensile				Compression		Tensile		Pressure	
	σ (MPa)	ε (%)	E (kPa)	T (MJ/m^3)	σ (MPa)	E (kPa)	GF	LOD (%)	(kPa^{-1})	
HAPAA/PANI	**0.90**	**2590**	**52.3**	**7.85**	**5.51**	**83.6**	**17.90**	**0.05**	**0.14**	**This work**
P(AAM-co-HEMA)/PANI	1.90	300	~250	~2.5	14.47	/	5.70	0.3	/	[1]
PAAM/SA/NaCl	0.65	2000	50.0	4.77	/	45	2.70	0.2	1.45	[2]
PVA/PEI	0.6	500	~560	/	/	/	22.00	/	/	[3]
PAA/TA@CNCs/Al^{3+}	0.31	2770	50.0	5.6	3.50	/	7.80	/	/	[4]
PVA/TA@talc	0.65	700	/	/	1.0		9.17	/	/	[5]
PAA/rGO/Fe^{3+}	0.4	650	/	/	~0.32	/	1.32	/	/	[6]
PAA/Fe_3O_4	0.035	1400	35.8	/	/	/	19.6	1.0	/	[7]
P(AAM-co-LMA)/LiCl	1.37	2058	57.3	8.66	3.85	/	5.44	0.25	0.13	[8]
PVA/PAA/CNTs	~0.026	550	/	/	/	/	1.61	/	0.243	[9]
PAAM/carrageenan	0.35	950	417	/	/	/	6.00	0.5	/	[10]
Gelatin/Na_3Cit	1.91	542	91.0	4.99	~1.5	~460	1.5	5.0	/	[11]
PAA/LM	1.26	~650	~150	3.54	/	/	1.54	/	/	[12]
Cellulose	0.016	129	21.0	/	~0.5	~40	0.3	/	/	[13]
P(AAM-co-HEMA)/LM	0.13	1500	24.0	0.98	0.35	/	/	/	1.43	[14]
HAPAM/CNC@CNTs	0.31	2900	17.4	3.60	1.10	/	7.63	0.2	/	[15]
ACC/PAA/SA	0.005	1000	/	/	0.004	/	/	/	0.17	[16]
PAA/PPy/Fe^{3+}	0.007	1500	/	/	0.06	800	/	/	/	[17]
PAA/PANI/Fe^{3+}	0.036	991	/	/	/	/	18.28	5.0	/	[18]
PVA/AgNWs	/	1000	/	/	/	/	2.25	/	/	[19]
PANIPAM/PANI	0.042	210	/	/	/	/	/	/	/	[20]
PVA/MXenes	0.035	350	/	/	0.11	/	44.85	1.0	/	[21]
PAAM/PEGDA/$MgCl_2$	~0.90	~650	~140	/	~0.1	/	/	/	/	[22]

Note: "/" means "not shown" in the reference.

S3. Supporting Figures

S3.1 The synthesis procedure of PAAN hydrogels

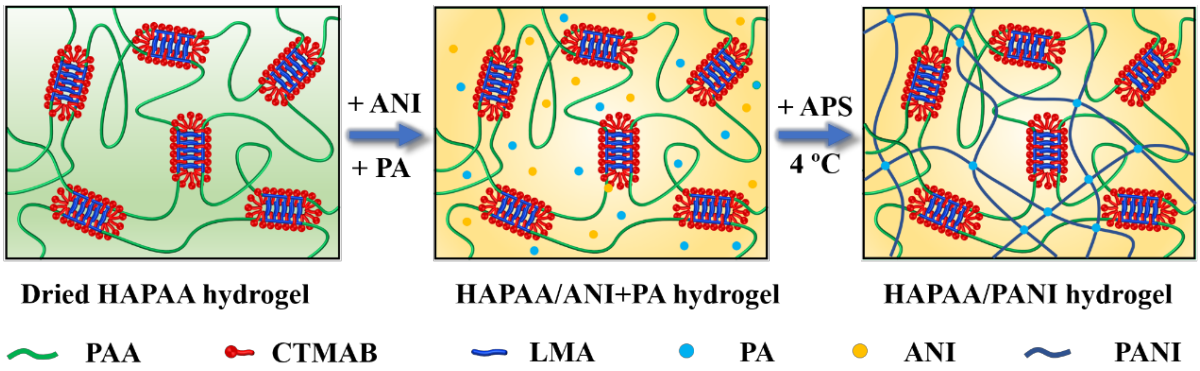

Figure S1. Schematic illustration of the synthesis process of the PAAN hydrogels by the pre-infiltration method.

In this work, we used a pre-infiltration method in the combination of the *in situ* polymerization to prepare the conductive DN PAAN hydrogels (Figure S1). At first, the hydrophilic monomer AA and a small amount of hydrophobic monomer LMA were dissolved in deionized water with the assistance of surfactant CTMAB. The water-insoluble LMA with a long side chain is dissolved in the wormlike surfactant micelles. After polymerization, these micelles were served as physical cross-linking points. The obtained pure HAPAA hydrogel plate was dried in the open air (RH ≈ 40%) at room temperature to a constant weight (~48 hours) at first (Figure S2a). Then the dried hydrogel was immersed into the ANI/PA solution to reswollen the dry gel. A large amount of ANI and PA molecules were absorbed into the HAPAA gel network as the color of the gel turns from transparent to light brown (the color of PA). According to the weight change curves of the HAPAA hydrogel during the reswelling process, the immersing time was controlled at 30 mins, which allows the hydrogels to reach their original weight (Figure S2b). Interestingly, we found that the HAPAA hydrogel showed a rapid absorption speed and swelled very unevenly when immersed in pure ANI aqueous solution (Figure S2c). After about 30 mins, the hydrogel was twisted and completely lost its mechanical properties (immediately fracture when stretched and can be easily crushed into small pieces by finger). After about three hours, the HAPAA hydrogel was totally disintegrated in an ANI solution. Thus, in this work, PA was not only used as the gelator and doping agent for PANI as previously reported but also served as a stabilizer to stabilize the HAPAA hydrogel network during the immersing process.

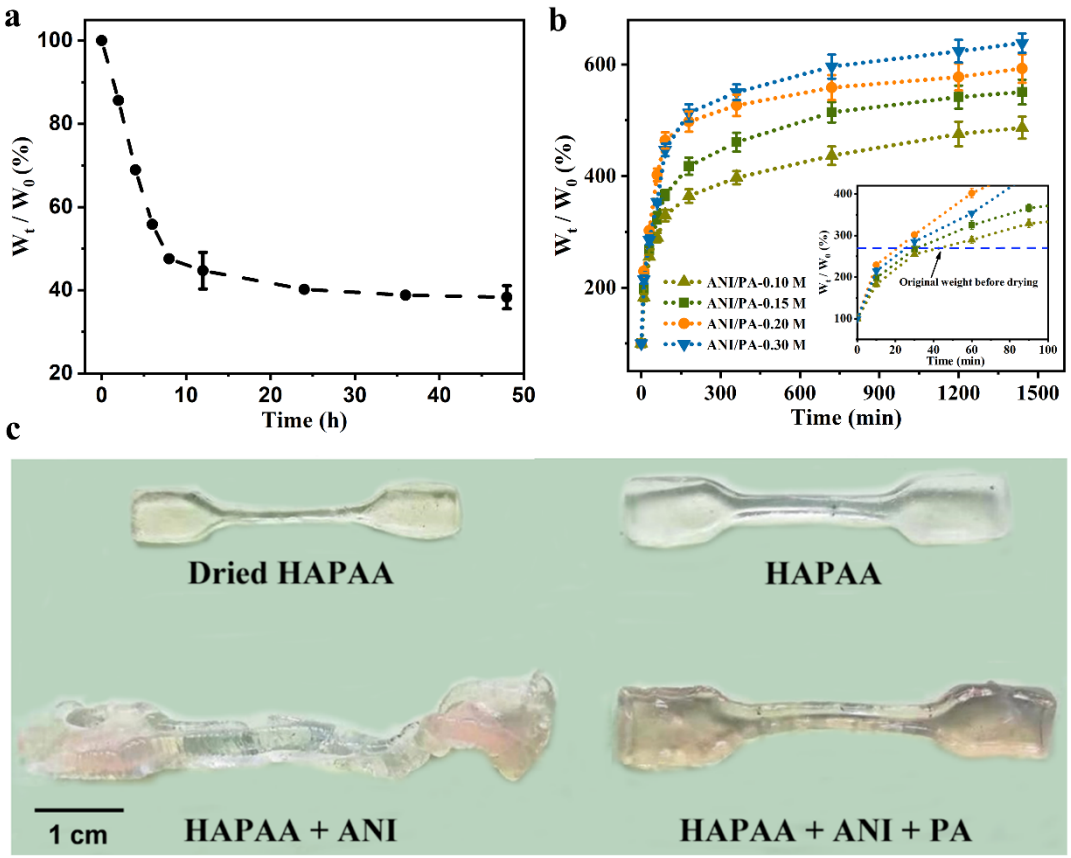

Figure S2. (a) the weight change ratio of the HAPAA hydrogel under ambient conditions. (b) The reswelling behavior of HAPAA hydrogel in ANI/PA aqueous solutions with different ANI concentrations. (c) The photographs of the as-prepared HAPAA hydrogel, the dried HAPAA hydrogel, the HAPAA hydrogels after reswelling in the ANI aqueous solution (30 min), and ANI/PA (30 min) solution, respectively.

S3.2 XRD characterization of PAAN hydrogel

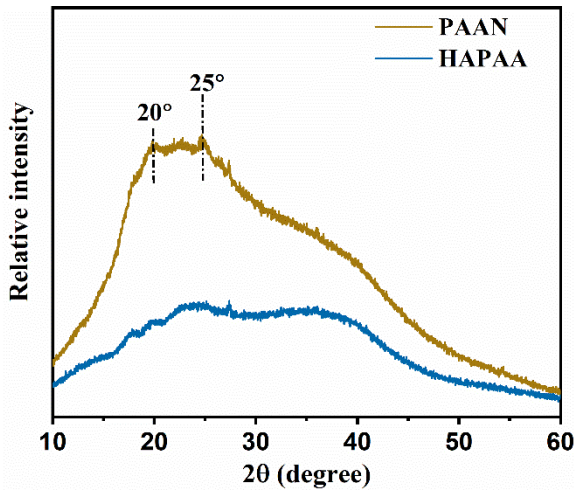

Figure S3. XRD patterns of the dehydrated HAPAA and PAAN hydrogels.

The XRD pattern of the dehydrated PAAN hydrogel shows two peaks at 20º and 25º, which can be attributed to the totally dried PANI and the wet PANI, respectively.[23] This indicates that the presence of PANI structures in the HAPAA network. In contrast, these two peaks were not observed for the dehydrated HAPAA hydrogel. The broad peak in HAPAA hydrogel can be attributed to the long-range ordering of the alkyl side chains of LMA units in the water-free core of the mixed micelles.[24]

S3.3 Swelling ratio and water content of PAAN hydrogel

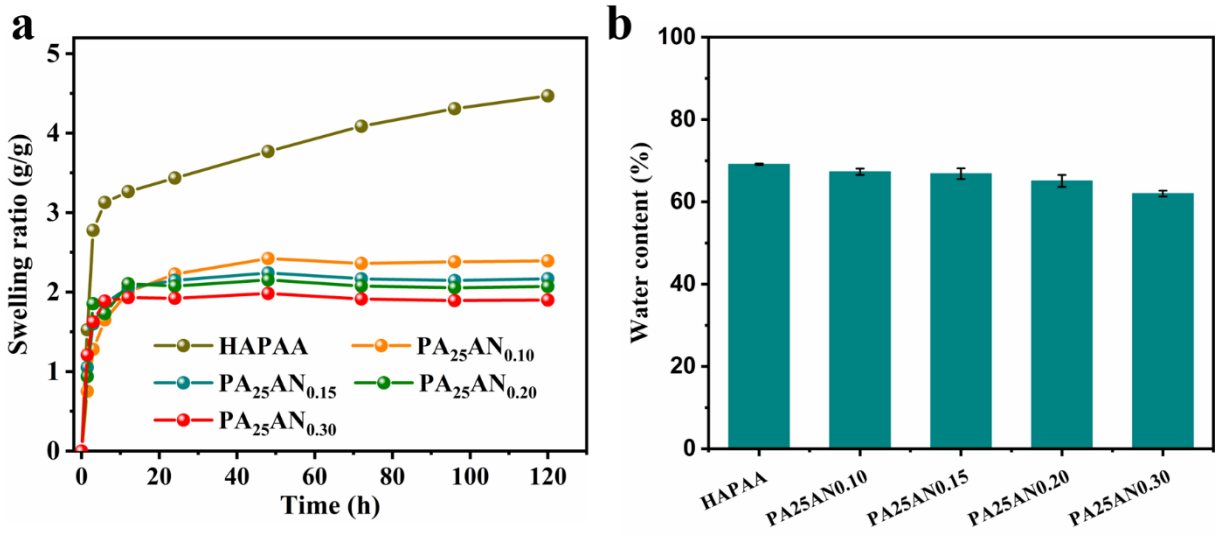

Figure S4. (a) Swelling ratio and (b) water content of the HAPAA and PAAN hydrogels.

S3.4 Microstructure and morphology of PAAN hydrogel

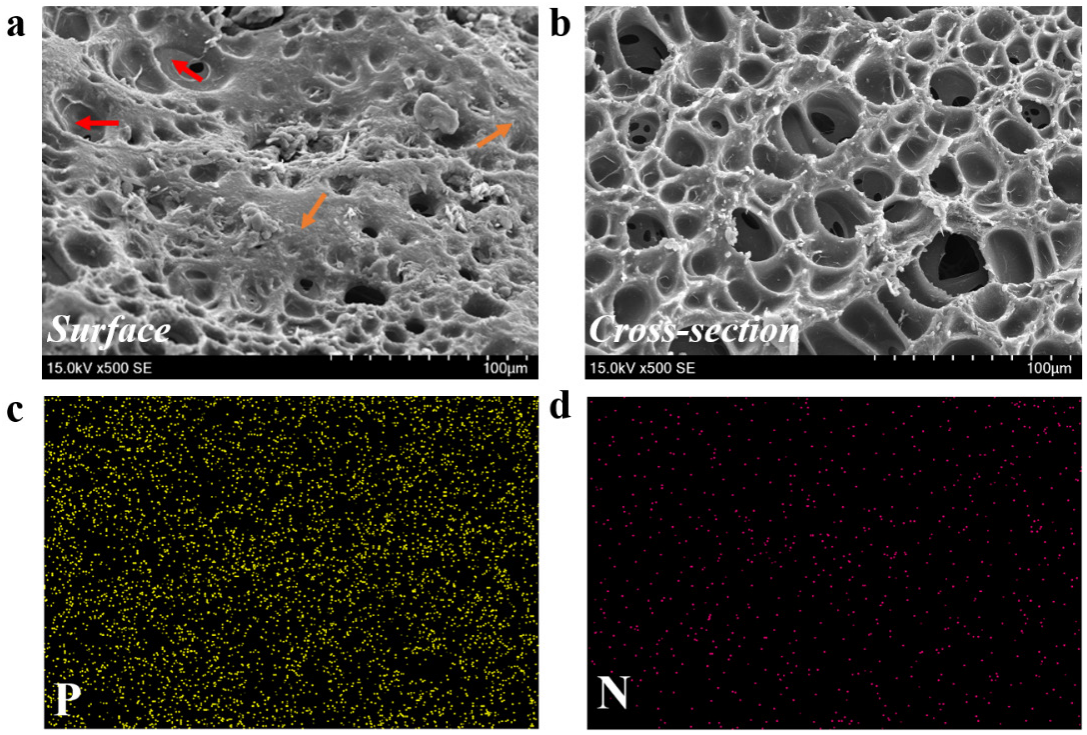

Figure S5. (a) The surface SEM image $PA_{25}AN_{0.15}$ hydrogel showing the PANI is formed inside the pores (red arrows) and on the surface (orange arrows) of the HAPAA hydrogel. (b) the cross-section SEM image shows that the PANI is interpenetrated within the branches of HAPAA hydrogel. (c) the corresponding EDS mapping images (elements: N and P) of the surface SEM image.

S3.5 Excellent mechanical property of PAAN hydrogel

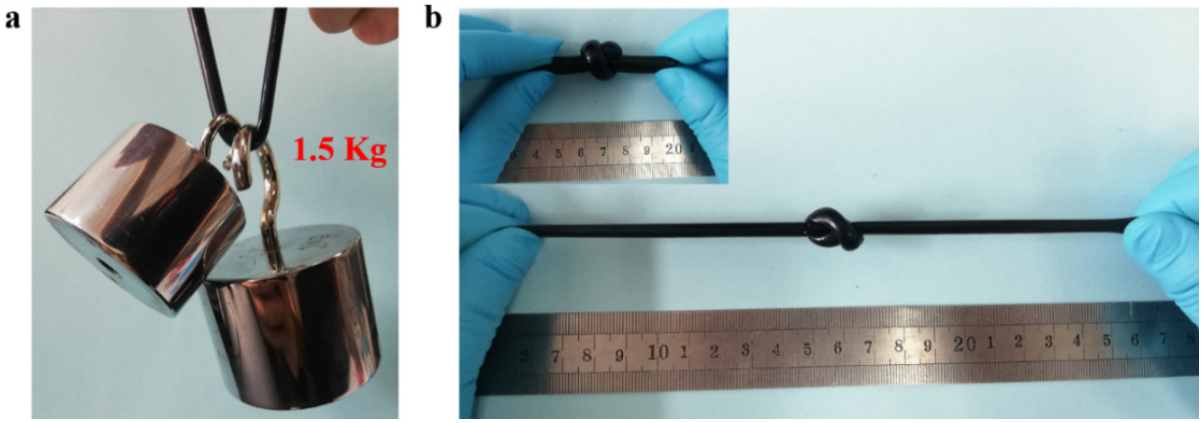

Figure S6. The excellent mechanical property of PAAN hydrogel. (a) The gel is capable of supporting a 1.5 Kg (about 800 times heavier than that its own weight) load without any apparent damage. (b) The gel can be knotted and then stretched to a very large strain.

S3.6 Influence of PANI contents on the compression performance of PAAN hydrogels

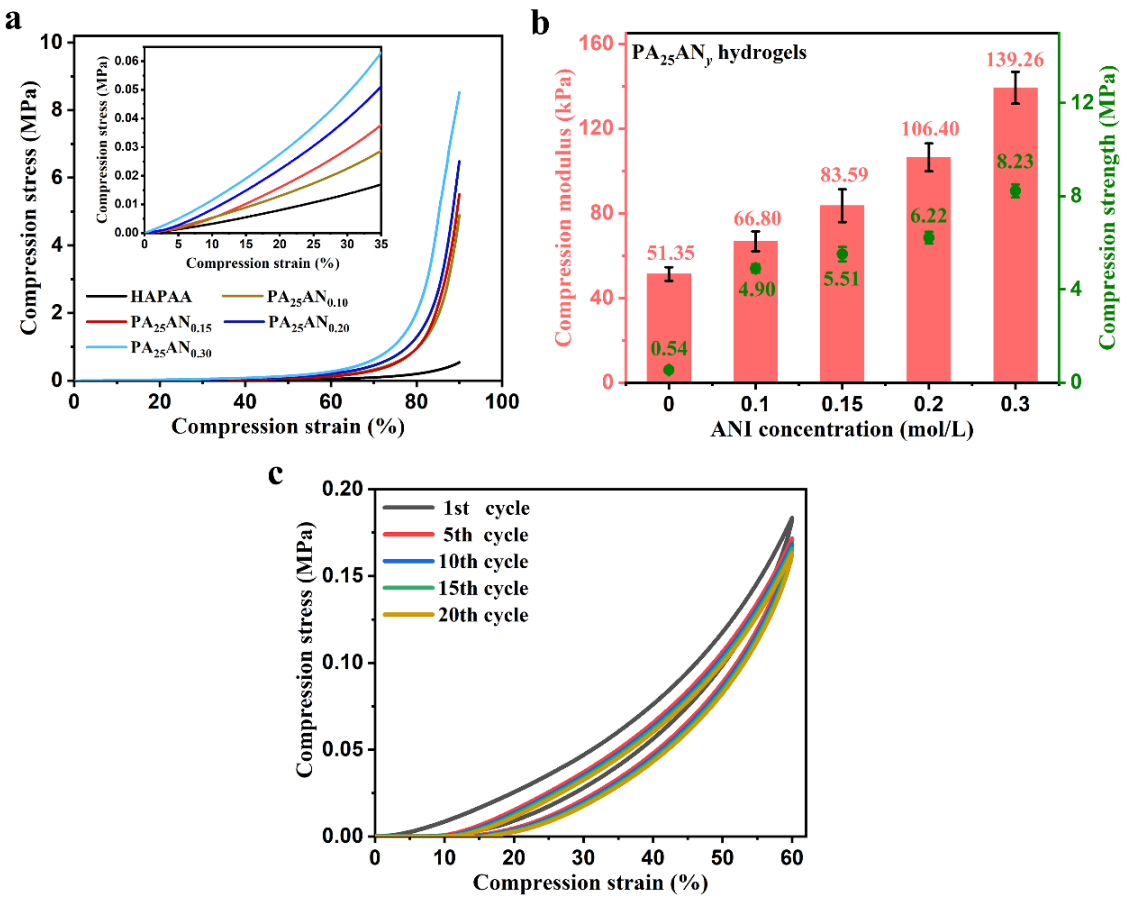

Figure S7. (a) Representative compression stress-strain curves of $PA_{25}AN_y$ hydrogels with different PANI contents. (b) the corresponding compression strength and modulus of $PA_{25}AN_y$ hydrogels calculated from Figure S6a. (c) Representative compressive cyclic tests (20 cycles) of $PA_{25}AN_{0.15}$ hydrogel.

The influence of PANI contents on the compression property of PAAN hydrogels was also investigated. It was found that all hydrogels can be compressed to 90% strain without fracture. The compression and modulus of $PA_{25}AN_y$ hydrogels were gradually enhanced with increasing the ANI concentration of the PANI precursor solution, demonstrating the efficient reinforcement effect of the PANI network. The compression strength of $PA_{25}AN_{0.30}$ hydrogel reached ~8.23 MPa, which is about 15 times higher than that of the pure HAPAA hydrogel and much higher than most of the reported hydrogen-based electronics (Table S4). Despite the high compression strength, $PA_{25}AN_y$ hydrogels showed moderate compression modulus less than 150 kPa, which is close to human muscle fibers and tendons. In addition, the PAAN hydrogel also exhibits excellent compression stability (Figure S7c)

S3.7 Optimization of AA contents in HAPAA hydrogel network

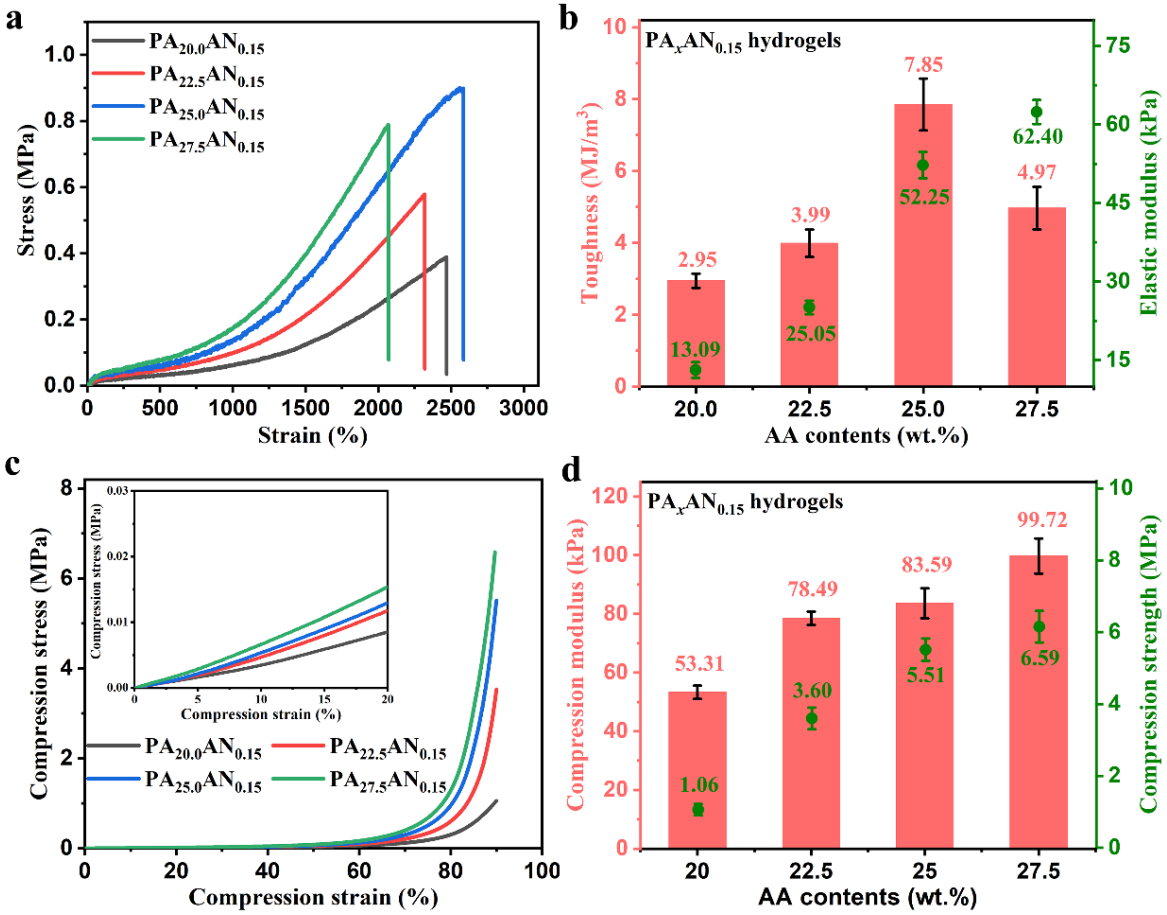

Figure S8. The AA contents in pure HAPAA hydrogel dramatically affect the mechanical behaviors of the $PA_xAN_{0.15}$ hydrogels. (a) Representative tensile stress-strain curves of $PA_xAN_{0.15}$ hydrogels with various AA (wt.%) contents. (b) The corresponding toughness and tensile elastic modulus of the gels. (c) Representative compression curves of $PA_xAN_{0.15}$ hydrogels. (d) The corresponding compression modulus and strength of the $PA_xAN_{0.15}$ hydrogels.

Mechanical properties of the $PA_xAN_{0.15}$ hydrogels were investigated to optimization the AA contents in the pure HAPAA hydrogel network. As shown in Figure S8a-b, the tensile property of $PA_xAN_{0.15}$ hydrogels gradually enhanced with the AA contents increased from 20.0 wt.% to 25.0 wt.%. The $PA_{25}AN_{0.15}$ exhibits an ultrahigh toughness of 7.85 MJ/m^3 and a moderate modulus of 52.25 kPa. However, when the AA contents further increased to 27.5 wt.%, the toughness decreased to 4.97 MJ/m^3. Moreover, the compression strength of $PA_xAN_{0.15}$ hydrogels gradually enhanced with the AA contents increased from 20 wt.% to 27.5 wt.%. The $PA_{27.5}AN_{0.15}$ hydrogel exhibits the highest compression strength and modulus of 6.59 MPa and 99.72 kPa, respectively (Figure S8c-d). The $PA_{25}AN_{0.15}$ hydrogel showed a relatively smaller compression strength and modulus of 5.51 MPa and 83.59 kPa. However, considering the highly desired high toughness and high strength, and low modulus for sensor materials, the optimum AA content of 25.0 wt.% can be determined.

S3.8 Microstructure of the PAAN hydrogel with high PANI content

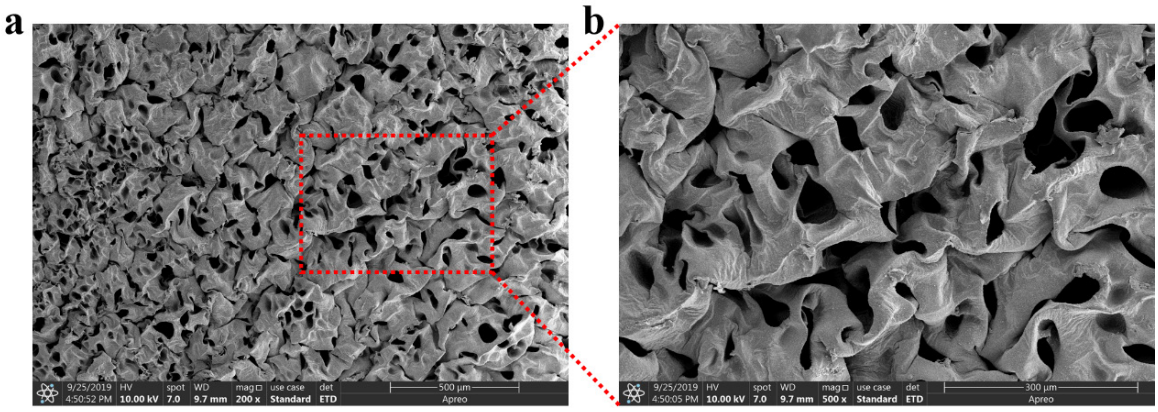

Figure S9. The cross-section SEM images of the $PA_{25}AN_{0.30}$ hydrogel show its compact structure and the dense PANI network.

S3.9 The notch-insensitivity and fracture energy of PAAN hydrogels

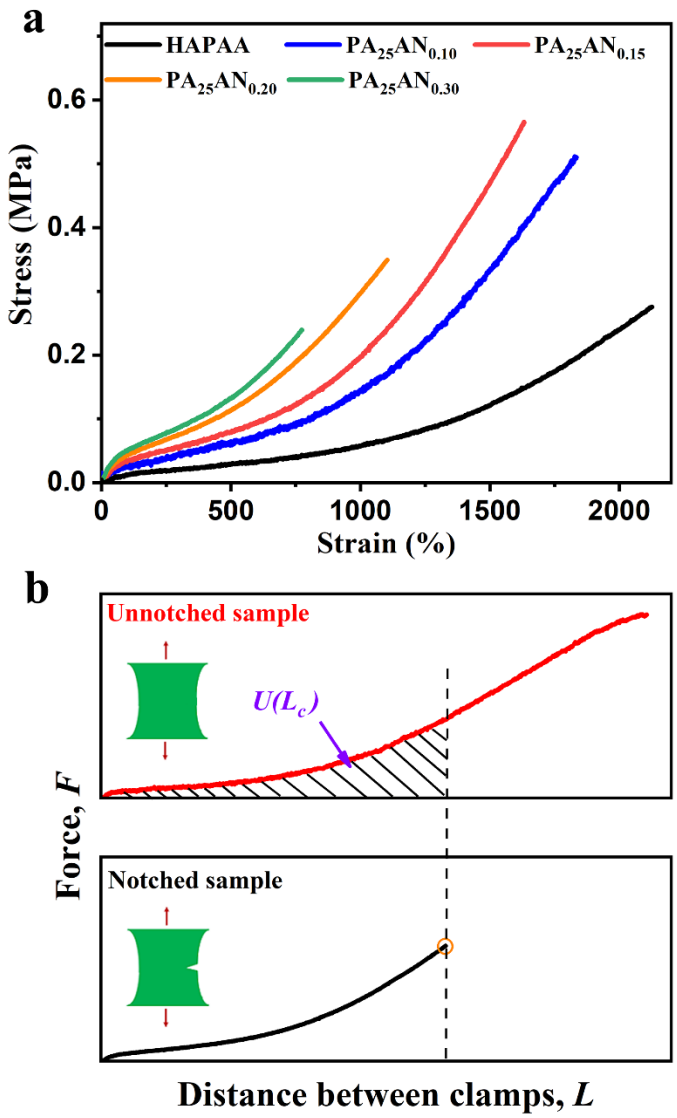

Figure S10. (a) The excellent notch-insensitivity of $PA_{25}AN_y$ hydrogels. (b) Experimental determination of fracture energy.

We adopted the single-notch method to evaluate the notch-insensitivity of our $PA_{25}AN_y$ hydrogels. Firstly, a pre-crack was cut using a surgical blade with an initial crack length of ~1 mm, which is about one-fourth of the width of the sample. Then, the notched samples were stretched with a constant speed of 100 mm min^{-1} in ambient air at room temperature. As shown in Figure S10a, all the $PA_{25}AN_y$ hydrogels with different PANI contents enjoy a good notch-insensitivity. The $PA_{25}AN_{0.15}$ hydrogel can still be stretched to more than 17 times its original length after notching. Even the $PA_{25}AN_{0.30}$ hydrogel, which exhibits the worst mechanical properties, enjoys a critical stretch (λ_c) larger than 8. When the notched sample is stretched, the high-stiffness PANI network is may sufficient to block the induced crack propagation, while the hydrophobic micelles and the dynamic interactions simultaneously break and dissipate strain energy. Based on the tensile curve of the notched sample, the fracture energy can be

calculated (Figure S10b). To measure the fracture energy, two samples of the same gel should be separately stretched. One sample was unnotched, and the other was notched. The unnotched sample was first stretched to record the force-length curve. When the two clamps were pulled to a distance L, the area beneath the force-length curve gave the work done by the applied force, $U(L)$. Then, the notched sample (the precise length of the notch is unimportant for this test) was stretched until the critical distance L_c, which is defined as the sample length when the notch turning into a running crack. In this work, the notch turned into the running crack at the end of stretching, and crack growth occurs just before the fracture of the notched gels. Hence, L_c was determined as the increase in the length at the end of the stretching process in the present work. The fracture energy was calculated from:

$$\Gamma = \frac{U(L_c)}{a_0 b_0}$$

where a_0 and b_0 represent the width and thickness of the sample, respectively. In our tests, a_0 = 4 mm, b_0 = 2 mm, and the initial sample length L_0 = 20 mm. The critical length (L_c) can be calculated as: $L_c = (\lambda_c - 1) \times L_0$. According to this method, the fracture energy of the $PA_{25}AN_y$ hydrogels can be obtained (Figure 2f in the main manuscript). The $PA_{25}AN_{0.10}$ and $PA_{25}AN_{0.15}$ hydrogels both possess ultrahigh fracture energy beyond 4100 J m^{-2}. Therefore, even though some mechanical damages such as scratching and notching were made on PAAN hydrogel, it continued to operate because the superior notch-insensitivity and high fracture energy can prevent damage from propagation under stretching, and thus buy some time for us to replace the sensor without interrupting its operation.

S3.10 The tunable mechanical properties of PAAN hydrogels

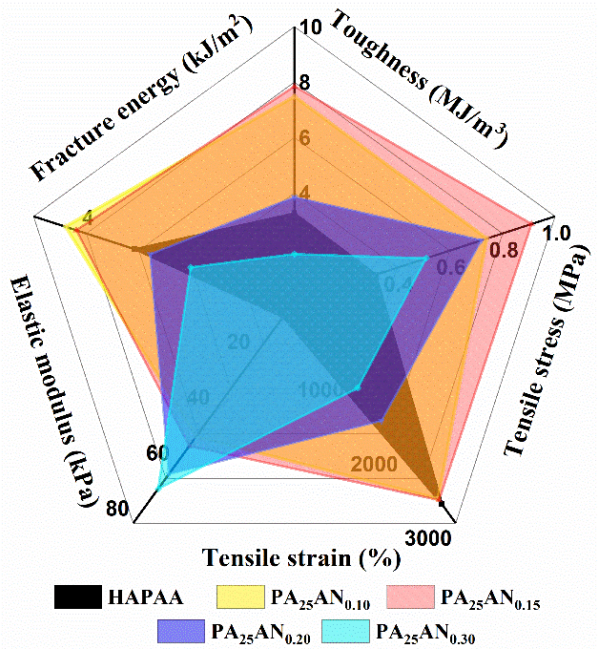

Figure S11. Spider chart representing the highly tunable mechanical performances of the $PA_{25}AN_y$ hydrogels. The $PA_{25}AN_{0.15}$ hydrogel shows well-balanced mechanical properties.

S3.11 The energy dissipation mechanism of PAAN hydrogel

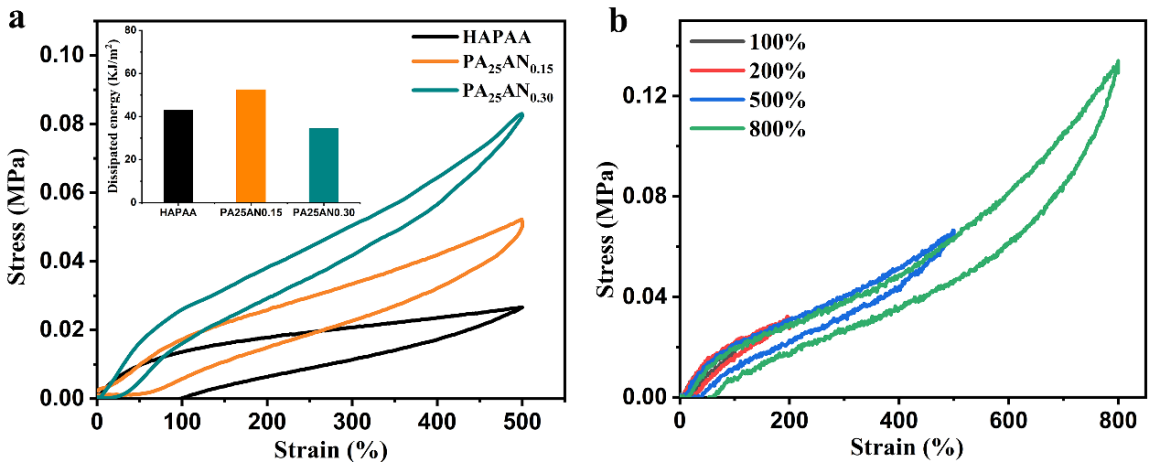

Figure S12. (a) Loading-unloading tensile curves of the pure HAPAA, $PA_{25}AN_{0.15}$, and $PA_{25}AN_{0.30}$ hydrogels at a strain of 500%. Inset picture shows the dissipated deformation energy calculated from the hysteresis loops. (b) Consecutive cyclic tensile loading-unloading curves of PAAN hydrogel under gradually increased strains (100%, 200%, 500%, and 800%).

The pure HAPAA hydrogel, the $PA_{25}AN_{0.15}$ hydrogel with the optimum mechanical property, and the $PA_{25}AN_{0.30}$ hydrogel with the worst mechanical property were chosen to perform cyclic tensile experiments to investigate the energy dissipation mechanism of PAAN hydrogel. The area between the loading and unloading curves gives the energy dissipated per unit volume. As shown in Figure S12a, the $PA_{25}AN_{0.15}$ hydrogel (~52 kJ m^{-3}) exhibited a bigger hysteresis loop comparing with the pure HAPAA hydrogel (~42 kJ m^{-3}). Nevertheless, the $PA_{25}AN_{0.30}$ hydrogel exhibited a much smaller hysteresis loop and exhibited an energy dissipation of ~37 kJ m^{-3}. Therefore, the proper content of PANI can enhance the energy dissipation ability of the HAPAA hydrogel, which is derived from the fracture of rigid PANI chains and the broken of dynamic interfacial interactions. However, an excessive amount of PANI would decrease the energy dissipation ability of PAAN hydrogel because the dense PANI network may hinder the disassociation of the hydrophobic micelles. Another possible reason is the high concentration of ANI/PA solution may lead to some micelles broken during the pre-infiltration process, as evidenced by the larger swelling ratio of HAPAA hydrogel in the pure ANI solution and in the ANI/PA solution of higher ANI concentration. Then, the PAAN hydrogel was stretched with a gradually increased strain (Figure S12b). As the strain increasing from 100% to 800%, a remarkable increase in the hysteresis loop can be observed since more PANI molecular chains break and more hydrophobic micelles and dynamic interfacial interactions disassociate. In addition, four loading curves are highly overlapped with no obvious Mullins effect can be observed, indicating the self-recovery of the gel network during the unloading processes, as a result of the re-associate of the broken hydrophobic micelles and the dynamic interfacial interactions. The small un-overlapped part of the loading curves probably can be ascribed to a small apart of the un-recoverable fracture of PANI chains.

S3.12 Tensile curves under different loading speeds

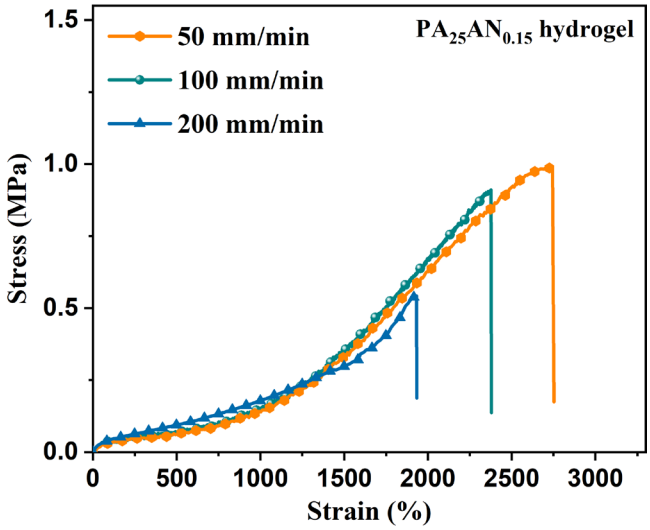

Figure S13. Tensile stress-strain curves of the $PA_{25}AN_y$ hydrogel with different loading speeds.

S3.13 The self-healing behavior of PAAN hydrogel

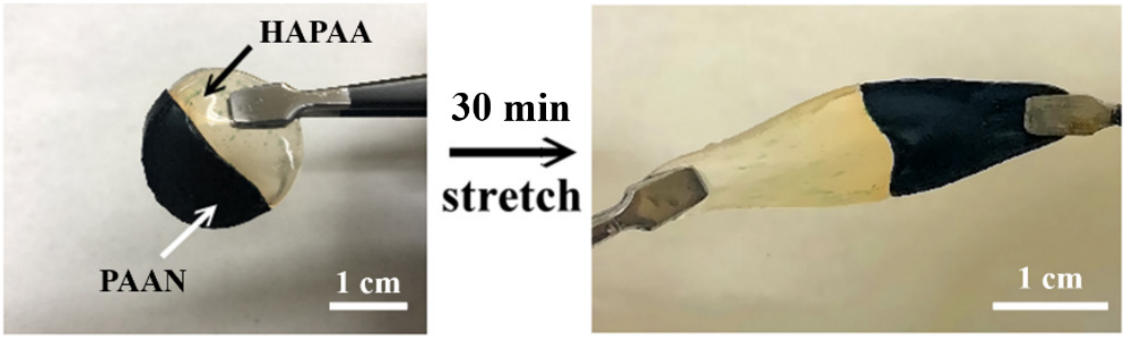

Figure S14. Photographs showing the self-healing behavior of the PAAN hydrogel. One part of the HAPAA semicircle sample was used to highlight the healing interface with the color difference.

S3.14 The surface morphology of the healed PAAN hydrogel

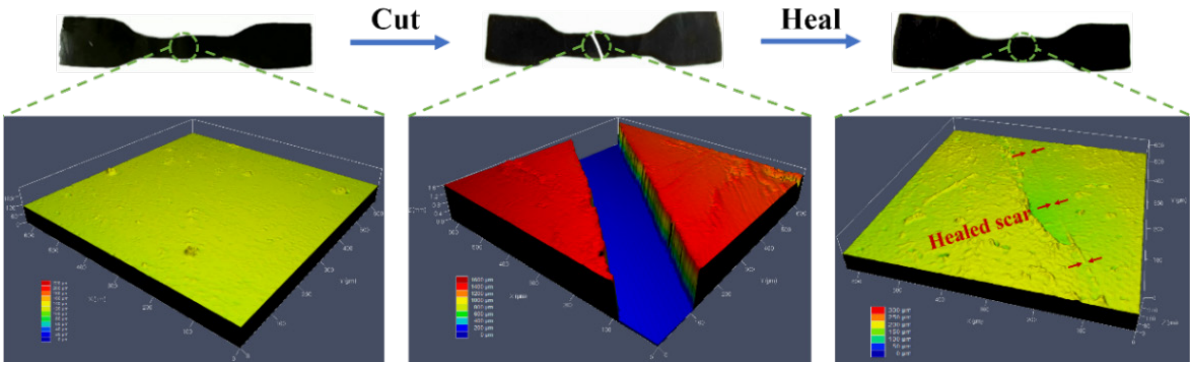

Figure S15. LCSM images of PAAN hydrogel before cut (left), after cut (middle), and after healed (right). The surface of the PAAN hydrogel before being cut is flat with no scar. When the sample was cut into two halves using surgical blades, a big gap existed between two separated parts. Then, the separated two parts were gently put into contact to allow them to self-healing. After 24 hours, the conspicuous damage on the sample was wholly healed except for leaving a vague scar.

S3.15 The remolding property of the PAAN hydrogel

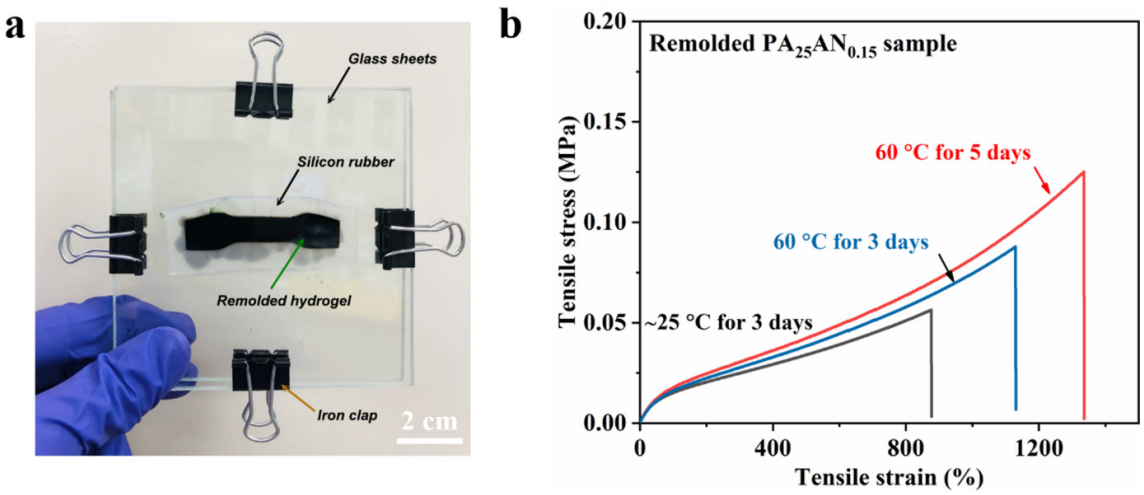

Figure S16. (a) The method for obtaining the remolded dumbbell-shape hydrogel sample for the tensile test. (b) Representative tensile stress-strain curves of the remolded $PA_{25}AN_{0.15}$ hydrogel sample at different temperatures and times.

Figure S16a shows the method for obtaining the remolded dumbbell-shaped PAAN hydrogel for the tensile test. Firstly, a dumbbell-shaped hydrogel sample was cut into small pieces, as shown in Figure 3b in the main manuscript. Then, all these small pieces were pressed into a silicon rubber mold with a dumbbell-shaped hollow that matches the dimensions of the original sample. Then, the rubber mold was sandwiched between two glass plates and clamped with iron clips to apply some pressure to the small pieces to allow them to merge into an integrated dumbbell-shape sample. The method to obtain the alphabet-shaped samples is quite similar, and the only difference is the silicon rubber molds with alphabet-shaped hollow were used. The remolded dumbbell-shape $PA_{25}AN_{0.15}$ hydrogels were subjected to tensile tests to evaluate their stretchability quantitatively. After three days at room-temperature (~25 °C, ~70% RH), the obtained $PA_{25}AN_{0.15}$ hydrogel exhibited an elongation at break of ~880% strain without any heat or light treatment, showing the excellent room-temperature remolding property of $PA_{25}AN_{0.15}$ hydrogel. Since increasing the temperature can facilitate the movement of the surfactant molecules and the reassociation of interfacial dynamic interactions, we also evaluated the influence of temperature on the tensile property of the remolded samples (**Figure S16b**). It was found that the sample can be stretched to ~1160% strain after remolding at 60 ºC for 3 days. Furthermore, the stretchability of the remolded hydrogel further increased to ~1340% after placing at 60 ºC for 5 days since increase remolding time leads to more broken micelles reassociate. When remolding at 60 ºC, the whole equipment was sealed in a PP bag and then immersed in a 60 ºC silicon oil. To obtain an accurate result, we also stored some water in the PP bag to evaluate the relative humidity in the PP bag up to ~100%; therefore, the water loss of the hydrogel during the remolding process can be minimized. After remolding, the weight decrease of the remolded sample is less than 5% compared with the original sample before the cutting.

S3.16 The influence of PANI contents on the self-healing ability of PAAN hydrogel

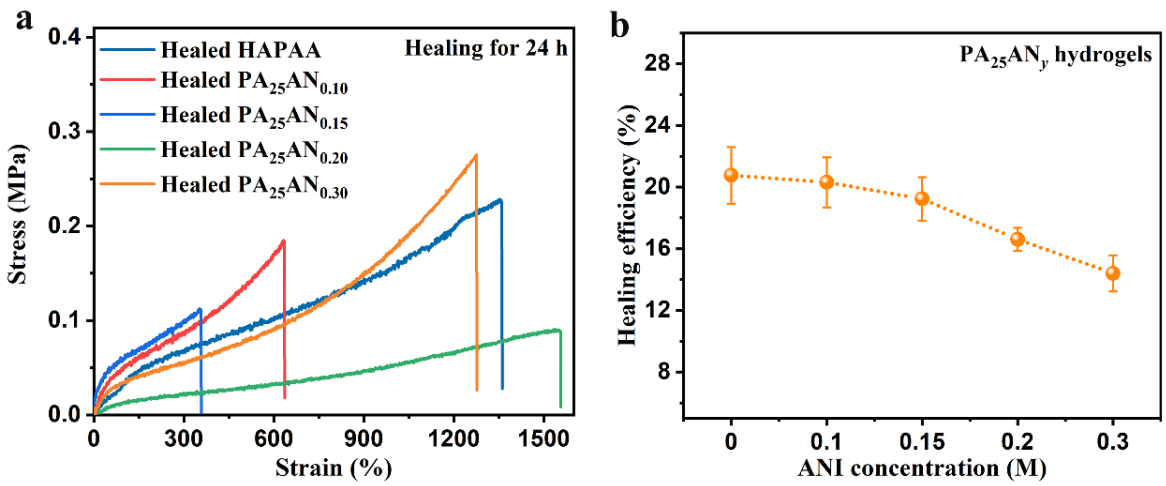

Figure S17. (a) The tensile curves of the healed HAPAA and $PA_{25}AN_y$ hydrogels. (b) Toughness healing efficiency of the HAPAA and $PA_{25}AN_y$ hydrogels in 24 h healing period.

Figure S17a shows the tensile curves of the HAPAA and $PA_{25}AN_y$ hydrogels with different PANI contents to investigate the influence of PANI content on the self-healing performance. For a reasonable comparison, the healing time for all the samples was controlled at 24 h (~25 °C, RH~70%). According to the tensile curves, toughness healing efficiency (defined as (T_h/T_0) ×100%, where T_h and T_0 are the toughness of the healed and original sample) can be accordingly calculated (**Figure S17b**). The $PA_{25}AN_{0.10}$ and $PA_{25}AN_{0.15}$ hydrogels with much higher mechanical strength showed approximate healing efficiency comparing with the pure HAPAA hydrogel. This can be attributed to a higher concentration of dynamic bonds on the cutting surface due to the existence of interfacial interactions between HAPAA and PANI networks, which can compensate for the negative effects of the increased mechanical strength on healing. Nevertheless, high PANI content will lead to a compact network structure and severely restrict the movement of HAPAA chains. Additionally, the dense PANI network may hinder the migration of the surfactant to the contact surface, resulting in a reduction in the number of the reassociated micelles (**Figure S9**). Therefore, $PA_{25}AN_{0.20}$ and $PA_{25}AN_{0.30}$ hydrogels showed a deteriorated healing efficiency given the same healing time.

S3.17 The self-healing mechanism of PAAN hydrogel

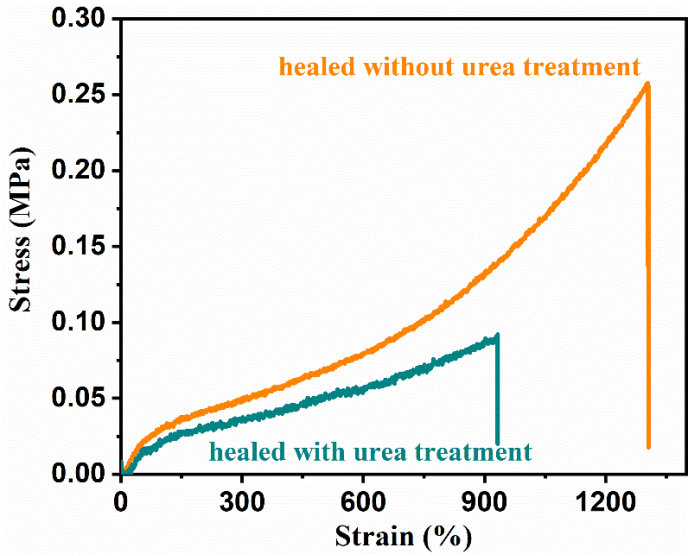

Figure S18. Tensile stress-strain curves for the $PA_{25}AN_{0.15}$ hydrogel after healing (red line) and without (black line) urea treatment.

The HAPAA hydrogel exhibits excellent self-healing property because the reversible cross-linking point (hydrophobic micelles) can reassociate after breaking. Introducing PANI hydrogel as the interpenetrating network in HAPAA hydrogel establishes dynamic interfacial hydrogen bonding and electrostatic interaction between two networks. We hypothesized that these dynamic interfacial interactions are also favorable for the self-healing of PAAN hydrogel. To verify this assumption, we first cut the dumbbell-like $PA_{25}AN_{0.15}$ hydrogel sample into two halves and then treat two cut surfaces with a small amount of urea solution (1 M) to inhibit the reassociation of hydrogen bonds.[25] Afterward, these two separated parts were brought into contact. After healing for 24 hours, the sample was subjected to stretch. The results showed that the urea-treated sample exhibited much lower tensile strain, strength, and modulus compared to the non-treatment sample. This observation verified that the dynamic interfacial interactions between two networks are conducive to the self-healing of PAAN hydrogel. Accordingly, the excellent self-healing ability of $PA_{25}AN_{0.10}$ and $PA_{25}AN_{0.15}$ hydrogels can be ascribed to the synergy effect enabled by the reversible hydrophobic micelles in the HAPAA network and the dynamic interfacial interactions between HAPAA and PANI networks.

S3.18 The multicycle self-healing ability of PAAN hydrogel

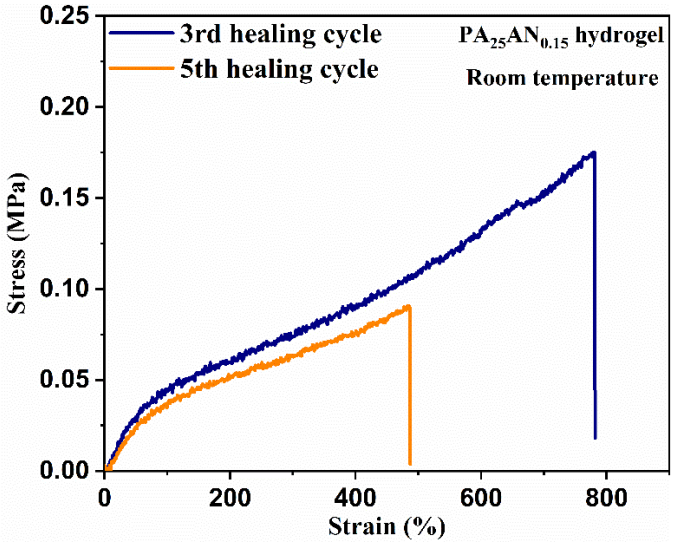

Figure S19. The tensile stress-strain curves of the $PA_{25}AN_{0.15}$ hydrogel after three and five successive healing cycles.

S3.19 The conductivity and electrical healing ability of PAAN hydrogels

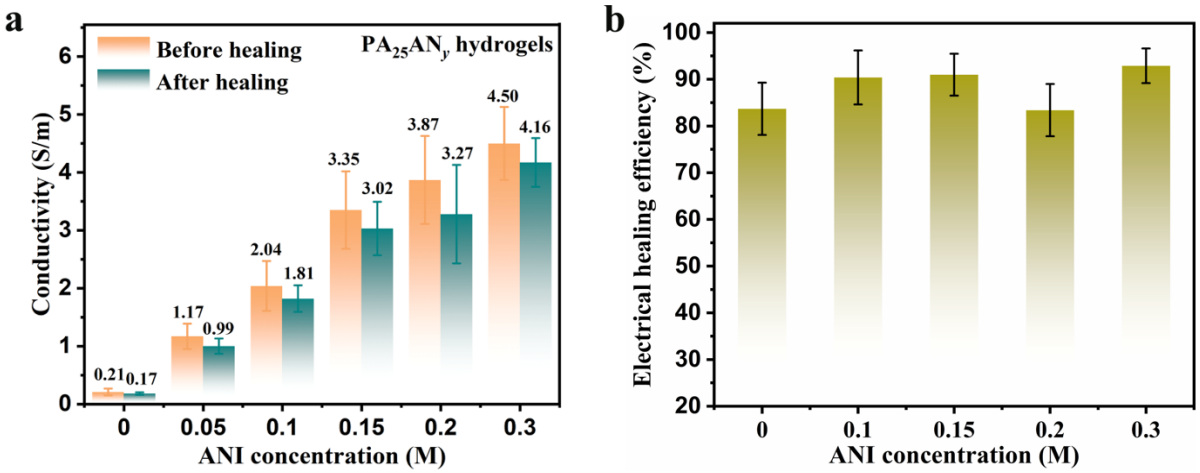

Figure S20. (a) The electrical conductivity of the HAPAA and $PA_{25}AN_y$ hydrogels before and after self-healing. (b) The electrical self-healing efficiency of HAPAA and $PA_{25}AN_y$ hydrogels.

S3.20 The method for measuring the strain and pressure sensitivity of PAAN hydrogels

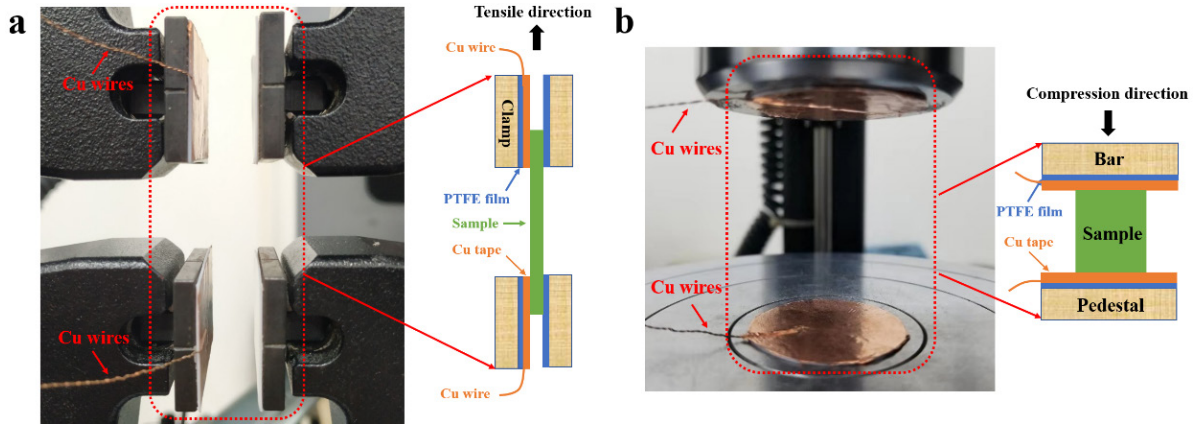

Figure S21. The photographs and schematic illustrations of the methods applied for the (a) tensile and (b) pressure sensory performance tests.

The methods for the tensile and pressure sensory performance tests are shown in Figure S20. These methods can minimize the change of contact resistance between the hydrogel sample and the electrode. **Figure S21a** shows the detailed photo and schematic illustration of the method for measuring the strain sensory performance**.** The tensile fixture was attached by PTFE film (as an insulator) and Cu tape (connected with a Cu wire). The configuration is a multilayer structure, from left to right is clamp, PTFE film, Cu tape, hydrogel sample, PTFE film, and clamp. **Figure S21b** shows a detailed photo of the device for pressure sensory performance tests. The configuration is also a multilayer structure, from bottom to top are pedestal, PTFE film, Cu tape, hydrogel sample, Cu tape, PTFE film, and compression bar. During tests, the Cu wires were connected with a Keithley 2601B source meter to collect data in-suit.

S3.21 The exceptional tensile and strain sensitivity of PAAN hydrogel strain sensor

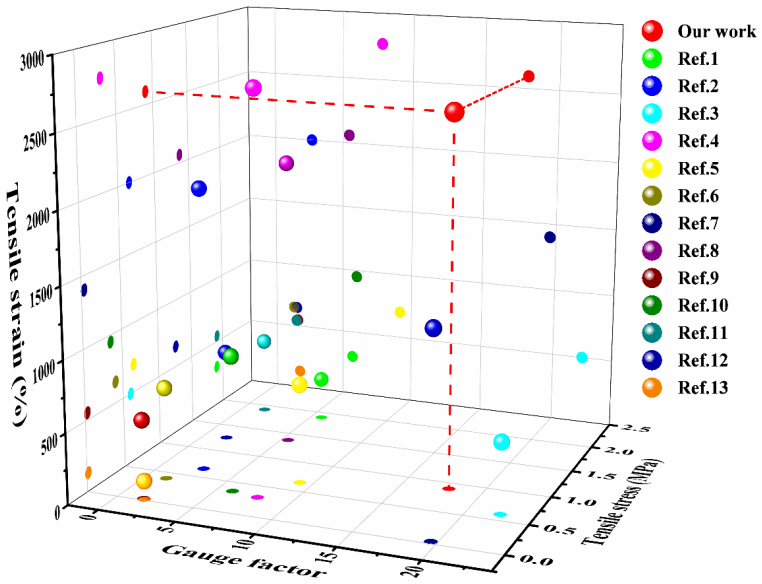

Figure S22. Graphic comparison of the maximum GF value and the mechanical property of $PA_{25}AN_{0.15}$ hydrogel strain sensor with other recently reported hydrogel sensors.

S3.22 The limitation of detection of the PAAN hydrogel pressure sensor

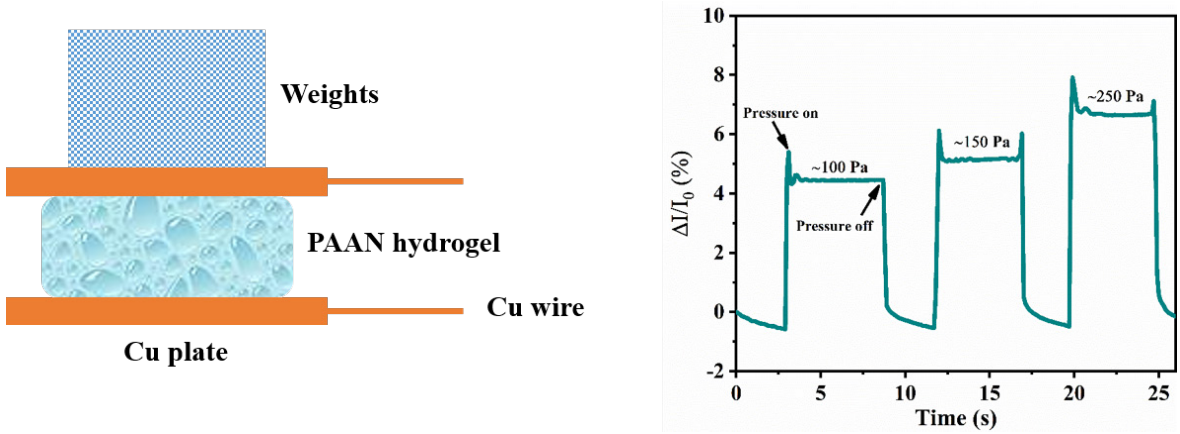

Figure S23. Response behavior of the PAAN hydrogel pressure sensor to different small pressures.

S3.23 The pulse monitoring by using PAAN hydrogel strain sensor

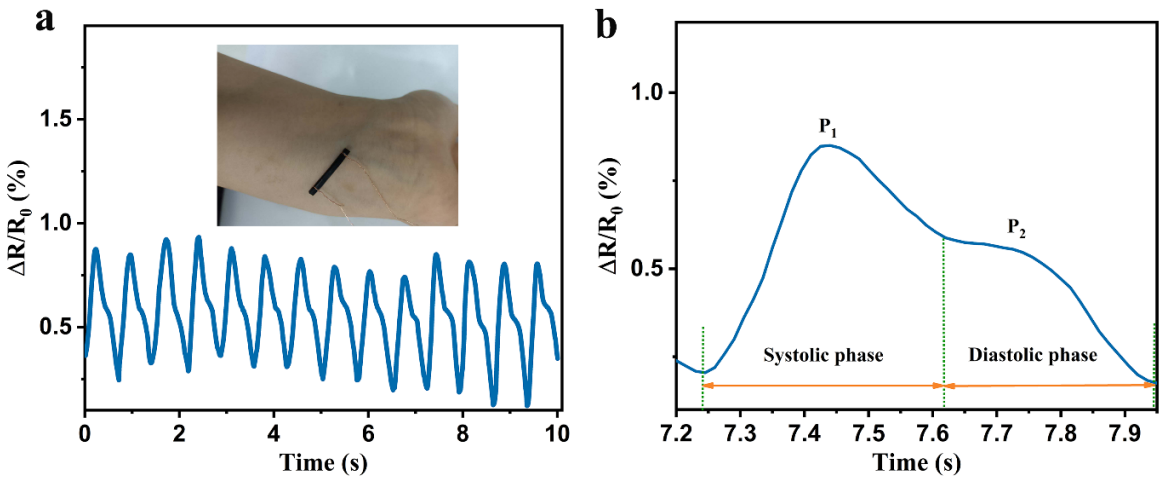

Figure S24. (a) The relative resistance change of the PAAN hydrogel in response to human pulse. The tester shows a pulse of ~80 cycles per minute. The inset picture shows the PAAN hydrogel strain sensor attached to the wrist where the pulse is strongest. (b) The magnification of a single period of the recorded pulse waveform.

S3.24 The handwriting monitoring ability of HAPAA hydrogel

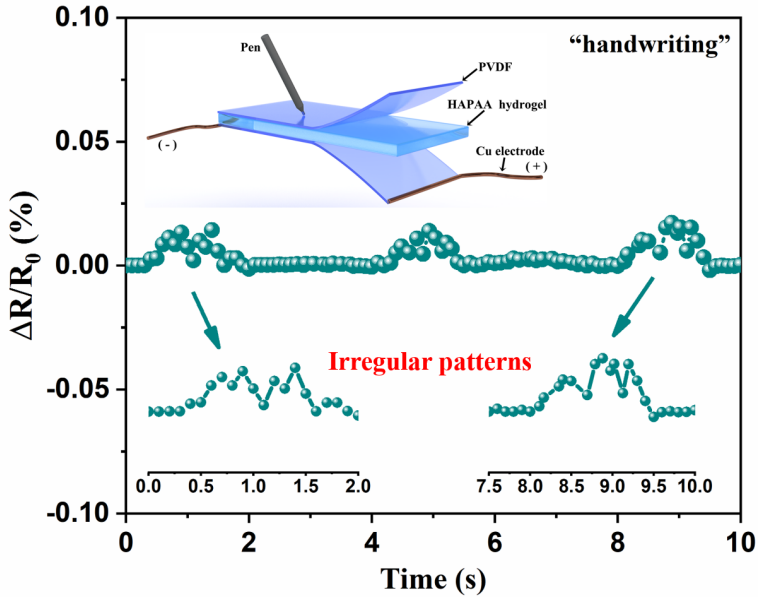

Figure S25. Relative resistance change ratio when writing "OK" on the HAPAA hydrogel screen. The HAPAA hydrogel screen produced irregular patterns when detecting handwriting signals.

S3.25 The artificial electronic skin application of PAAN hydrogel

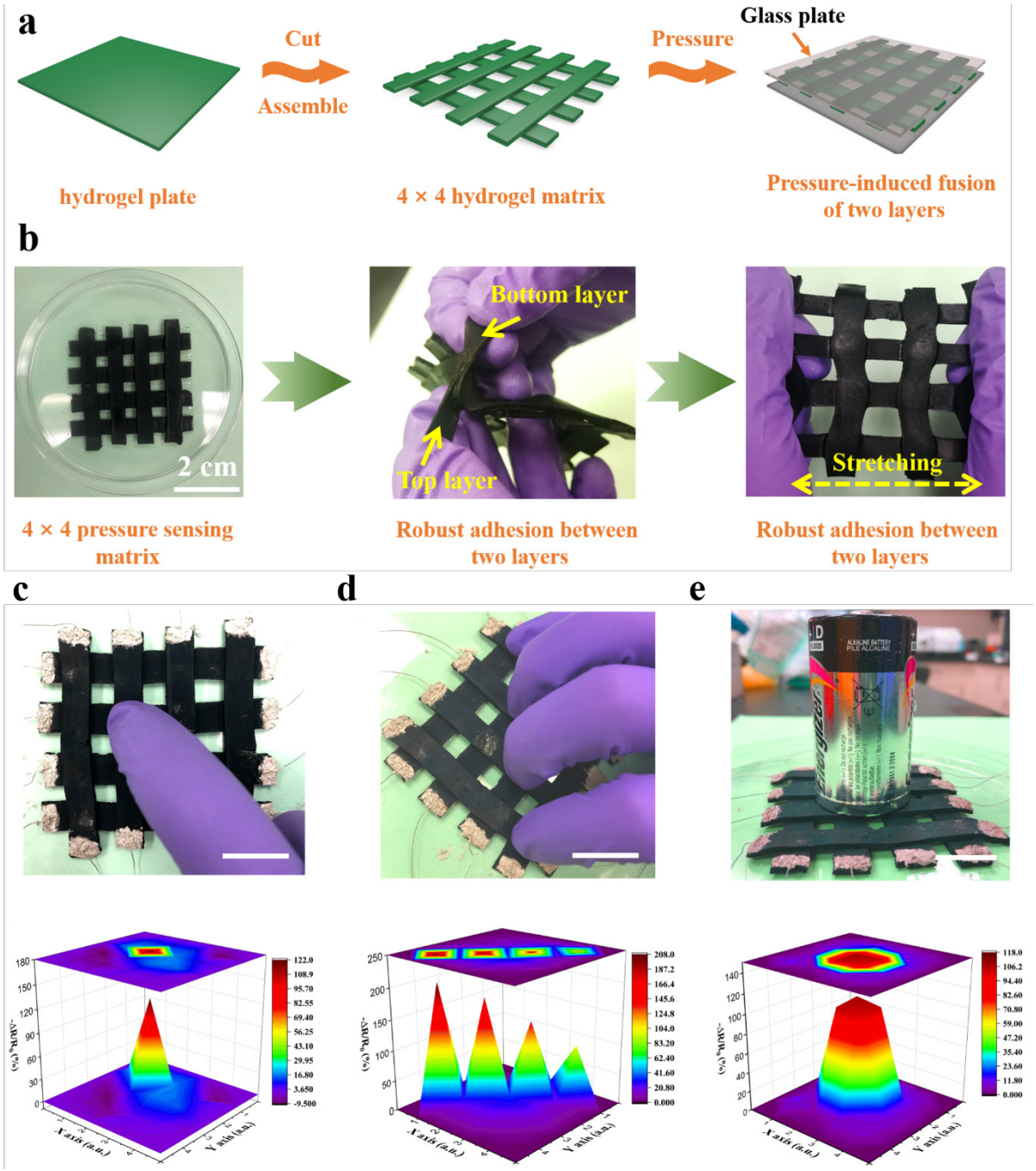

Figure S26. (a) Schematics show the fabrication processes of the PAAN hydrogel electronic skin. (b) Pictures of the fabricated electronic skin and its robust adhesion between two layers. (c-e) Pictures show fingers and a battery pressed on the artificial electronic skin, and the 3D maps show the corresponding detected pressure magnitude and distribution.

S4. Supporting References

[1] Z. Wang, J. Chen, Y. Cong, H. Zhang, T. Xu, L. Nie, J. Fu, *Chem. Mater.* **2018**, 30, 8062.

[2] X. Zhang, N. Sheng, L. Wang, Y. Tan, C. Liu, Y. Xia, Z. Nie, K. Sui, *Mater. Horiz.* **2019**, 6, 326.

[3] C. Wang, K. Hu, C. Zhao, Y. Zou, Y. Liu, X. Qu, D. Jiang, Z. Li, M.-R. Zhang, Z. Li, *Small* **2020**, 16, 1904758.

[4] C. Shao, M. Wang, L. Meng, H. Chang, B. Wang, F. Xu, J. Yang, P. Wan, *Chem. Mater.* **2018**, 30, 3110.

[5] X. Pan, Q. Wang, R. Guo, Y. Ni, K. Liu, X. Ouyang, L. Chen, L. Huang, S. Cao, M. Xie, *J. .Mater. Chem. A* **2019**, 7, 4525.

[6] X. Jing, H.-Y. Mi, X.-F. Peng, L.-S. Turng, *Carbon* **2018**, 136, 63.

[7] L. M. Zhang, Y. He, S. Cheng, H. Sheng, K. Dai, W. J. Zheng, M. X. Wang, Z. S. Chen, Y. M. Chen, Z. Suo, *Small* **2019**, 15, 1804651.

[8] S. Xia, Q. Zhang, S. Song, L. Duan, G. Gao, *Chem. Mater.* **2019**, 31, 9522.

[9] G. Ge, W. Yuan, W. Zhao, Y. Lu, Y. Zhang, W. Wang, P. Chen, W. Huang, W. Si, X. Dong, *J. Mater. Chem. A* **2019**, 7, 5949.

[10] J. Wu, Z. Wu, X. Lu, S. Han, B.-R. Yang, X. Gui, K. Tao, J. Miao, C. Liu, *ACS Appl. Mater. Inter.* **2019**, 11, 9405.

[11] Z. Qin, X. Sun, H. Zhang, Q. Yu, X. Wang, S. He, F. Yao, J. Li, *J. Mater. Chem. A* **2020**, 8, 4447.

[12] J. Xu, Z. Wang, J. You, X. Li, M. Li, X. Wu, C. Li, *Chem. Eng. J* **2020**, 392, 123788.

[13] R. Tong, G. Chen, D. Pan, H. Qi, R. A. Li, J. Tian, F. Lu and M. He, *Biomacromolecules* **2019**, 20, 2096.

[14] H. Peng, Y. Xin, J. Xu, H. Liu, J. Zhang, *Mater. Horiz.* **2019**, 6, 618.

[15] G. Su, J. Cao, X. Zhang, Y. Zhang, S. Yin, L. Jia, Q. Guo, X. Zhang, J. Zhang, T. Zhou, *J. .Mater. Chem. A* **2020**, 8, 2074.

[16] Z. Lei, Q. Wang, S. Sun, W. Zhu, P. Wu, *Adv. Mater.* **2017**, 29, 1700321.

[17] M. A. Darabi, A. Khosrozadeh, R. Mbeleck, Y. Liu, Q. Chang, J. Jiang, J. Cai, Q. Wang, G. Luo, M. Xing, *Adv. Mater.* **2017**, 29,1700533.

[18] G. Ge, Y. Lu, X. Qu, W. Zhao, Y. Ren, W. Wang, Q. Wang, W. Huang, X. Dong, *ACS Nano* **2020**, 14, 218.

[19] G. Cai, J. Wang, K. Qian, J. Chen, S. Li, P. S. Lee, *Adv. Sci.* **2017**, 4, 1600190.

[20] Z. Wang, H. Zhou, W. Chen, Q. Li, B. Yan, X. Jin, A. Ma, H. Liu and W. Zhao, *ACS Appl. Mater. Inter.* **2018**, 10, 14045.

[21] H. Liao, X. Guo, P. Wan, G. Yu, *Adv. Funct. Mater.* **2019**, 29, 1904507.

[22] X.-Y. Yin, Y. Zhang, X. Cai, Q. Guo, J. Yang and Z. L. Wang, *Mater. Horiz.* **2019**, 6, 767-780.

[23] L. Pan, G. Yu, D. Zhai, H. R. Lee, W. Zhao, N. Liu, H. Wang, B. C.-K. Tee, Y. Shi, Y. Cui, Z. Bao, *Proc. Natl. Acad. Sci. U.S.A.* **2012**, 109, 9287.

[24] V. Can, Z. Kochovski, V. Reiter, N. Severin, M. Siebenbu¨rger, B. Kent, J. Just, J. P. Rabe, M. Ballauff and O. Okay, *Macromolecules* **2016**, 49, 2281–2287.
[25] T. Wang, Y. Zhang, Q. Liu, W. Cheng, X. Wang, L. Pan, B. Xu, H. Xu, *Adv. Funct. Mater.* **2018**, 28, 1705551.